



Cite this: DOI: 10.1039/c7ta07117e

Tailoring pore structures to improve the permselectivity of organosilica membranes by tuning calcination parameters†

Huating Song,^a Yibin Wei^{ab} and Hong Qi^{*a}

Although microporous organosilica membranes have proven their excellent hydrothermal stability and permeability in H₂/CO₂ separation, it is still challenging to meet the permselectivity requirements of industrial applications. In this work, microstructures of 1,2-bis(triethoxysilyl)ethane (BTESE)-derived organosilica membranes were tailored through the tuning of calcination parameters including calcination temperature (T_c), heating rate (r) and dwelling time (t). A series of organosilica powders were prepared to optimize the calcination conditions for fabricating BTESE-derived organosilica membranes with excellent H₂/CO₂ separation performance. It is found that the organic bridge groups in organosilica networks are sensitive to calcination conditions. The organosilica membranes calcined at 600 °C with an expeditious calcination ($r = 10$ °C min⁻¹, $t = 5$ min) show a high cross-linking degree in their network and contain a high content of organic bridge groups. This expeditious calcination enables organosilica membranes to have a H₂ permeance of 4.61×10^{-8} mol m⁻² s⁻¹ Pa⁻¹ and a H₂/CO₂ permselectivity of 17.5. The organosilica membrane calcined at 600 °C with a slow calcination has a high H₂/CO₂ permselectivity of 36.4. The mechanisms of using expeditious or slow calcinations for developing organosilica membranes with outstanding separation performance are further confirmed, which may offer a novel method for preparing desirable organosilica membranes.

Received 11th August 2017
Accepted 23rd October 2017

DOI: 10.1039/c7ta07117e

rsc.li/materials-a

1. Introduction

Amorphous silica membranes which contain irregular pores with a size in the sub-nanometer level are some of the most important members in the inorganic microporous membrane family.¹ Due to their high permeability and molecular sieving capability, amorphous silica membranes are widely used in applications such as pervaporation²⁻⁴ and gas separation at high temperatures.^{2,5,6}

Hydrogen is a clean energy carrier which is mainly produced from methane steam reforming and water gas shift reactions.^{5,7} An effective *in situ* separation of H₂ and CO₂ is critical for efficient H₂ production and CO₂ capture. During the past few decades, a vast variety of silica-based membranes have been developed and used for H₂ and CO₂ separation.^{2,8-11} These membranes can be prepared by depositing an ultrathin and defect-free silica separation layer on a porous support. Ultrathin silica membranes that always exhibit acceptably high

permeance (10^{-8} to 10^{-6} mol m⁻² s⁻¹ Pa⁻¹) are usually fabricated through chemical vapor deposition (CVD) and sol-gel methods.^{1,5}

However, to efficiently separate H₂/CO₂, a silica membrane must show simultaneously high H₂ permeance and H₂/CO₂ permselectivity. Generally, sol-gel derived silica membranes show higher permeance but lower permselectivity than those of CVD derived silica membranes due to their looser porous structure.¹ Additionally, compared with CVD, the sol-gel technique has the advantages of low-cost, ease of control and assembly capability at the molecular scale. Therefore, the sol-gel technique is more widely used to prepare silica membranes for H₂/CO₂ separation.

For sol-gel derived silica membranes, tetraethoxysilane (TEOS) is typically used as a precursor, but they are unstable under hydrothermal conditions.¹² Besides, a series of bridged silsesquioxanes (O_{1.5}Si-R-SiO_{1.5}, R represents an organic bridge group), including bis(triethoxysilyl)methane (BTESM), 1,2-bis(triethoxysilyl)ethane (BTESE), 1,8-bis(triethoxysilyl)octane (BTESO), bis(triethoxysilyl)benzene (BTESB) and 1,2-bis(triethoxysilyl)acetylene (BTESA), *etc.*,¹³⁻¹⁵ could be used to prepare silica-based membranes as well. Because hydrothermal stability is another crucial criterion for silica-based membranes in practical H₂/CO₂ separation applications, among those organosilica membranes based on bridged silsesquioxane, BTESE-derived membranes have proven themselves as good

^aState Key Laboratory of Material-Oriented Chemical Engineering, Membrane Science and Technology Research Center, Nanjing Tech University, Nanjing 210009, Jiangsu, China. E-mail: hqi@njtech.edu.cn; Tel: +86-25-83172279

^bDepartment of Environmental Sciences, Macquarie University, Sydney, NSW 2109, Australia

† Electronic supplementary information (ESI) available. See DOI: 10.1039/c7ta07117e

candidates for H₂/CO₂ separation as they also exhibit unique hydrothermal stability.^{16,17}

Nevertheless, the permselectivity of BTESE-derived organosilica membranes for gas mixtures of H₂/CO₂ is still unsatisfactory.^{17,18} To improve the permselectivity of BTESE-derived organosilica membranes, many efforts have been made to tailor the structure of the organosilica membranes in the sol synthesis process, including changing the organic bridge groups,¹⁴ optimizing the sol synthesis parameters^{18,19} and incorporating metal into the network.^{20,21} In our previous studies, we have attempted to improve the H₂/CO₂ permselectivity of organosilica membranes by optimizing the sol synthesis parameters²² and by doping with metals (Zr and Nb).^{20,23} Moreover, Castricum *et al.* also found that the permselectivity of organosilica membranes can be significantly improved when the relative humidity of the supports decreases from 90% to <0.5%.¹⁹

Calcination is an indispensable process in the fabrication of BTESE-derived membranes since it is carried out to enhance the condensation reaction (Si–OH groups condense to form a Si–O–Si network) that increases the cross-linking degree of the silica network structure.²⁴ The cross-linking degree of the silica network is closely related to the pore structure of silica-based membranes. BTESE-derived membranes have hierarchically porous structures (Fig. 1). The internal pores are formed as network structures which contain Si–O–Si and Si–CH₂–CH₂–Si groups. Owing to the low cross-linking degree, there are also unconnected pores formed as spaces between the sol/gel particles, which are harmful to the permselectivity. Thus, the pore structure of the BTESE-derived membranes could be controlled by changing the calcination parameters. This might be an efficient way to improve the permselectivity of organosilica membranes.

In this work, we systematically investigate the influence of calcination parameters (*i.e.* calcination temperature, heating rate and dwelling time) on the porosity and chemical structure of BTESE-derived organosilica powders. Subsequently, the gas permeances of the organosilica membranes prepared with different calcination parameters were measured and compared.

The pore sizes and gas transport behaviors of the membranes were also discussed to shed further light on the effects of calcination parameters on the gas separation performance of the membranes.

2. Experimental

2.1. Chemicals

1,2-Bis(triethoxysilyl)ethane (BTESE, a purity of 97%) from ABCR was selected as the precursor. Ethanol (EtOH) was purchased from Merck. They were used as received without any further purification. Nitric acid (HNO₃, 65 wt%) was purchased from Lingfeng in Shanghai. Prior to further use, the concentrated nitric acid was diluted to 0.1 M with deionized water. Home-made γ -Al₂O₃ mesoporous membranes (pore diameter of 3–5 nm) were used as the support.

2.2. Preparation of the sols, gels and membranes

Organosilica sols were prepared in a clean room (class 1000 conditions) to avoid dust contamination. The details of the synthesis procedure for the organosilica sols are described in the ESI.† Briefly, the composition of the BTESE sol is BTESE : EtOH : H₂O : HNO₃ = 1 : 19.6 : 22.24 : 0.04 (molar ratio). Organosilica gels were obtained by drying the corresponding sols for 12 h in Petri dishes at room temperature. The obtained gels were then ground into fine powders. After that, the powders were calcined under a N₂ atmosphere with different calcination conditions which are given in Table S1.†

To prepare the BTESE-derived organosilica membranes, the same BTESE sol was diluted to a solution of 0.17 M Si in concentration. Then, the diluted sol was coated on home-made γ -Al₂O₃ mesoporous membranes through a dip-coating method. Subsequently, the membranes were calcined under a N₂ atmosphere. Four BTESE-derived membranes were prepared following the same calcination conditions used for powders P2, P6, P8 and P9 (see Table S1†). The four membranes are marked as M1 ($T_c = 400$ °C, $r = 0.5$ °C min⁻¹, $t = 180$ min), M2 ($T_c = 600$ °C, $r = 0.5$ °C min⁻¹, $t = 180$ min), M3 ($T_c = 600$ °C, $r = 10$ °C min⁻¹, $t = 180$ min) and M4 ($T_c = 600$ °C, $r = 10$ °C min⁻¹, $t = 5$ min), respectively. The calcination for all the organosilica powders and membranes was conducted in a tube furnace (GHA 12/1050, Carbolite).

2.3. Characterization of the gels and membranes

Fourier transform infrared (FTIR) spectroscopy (NICOLET 8700, Thermo Nicolet Corporation) tests were conducted to verify the chemical structure of the powders with KBr as the reference. N₂ adsorption–desorption isotherms at 77 K were conducted with a physical gas sorption instrument (ASAP 2460, Micromeritics). Prior to measurements, the samples were degassed under vacuum at 373 K for 12 h. The calculation of the pore size distributions was performed by applying the non-local density functional theory (NLDFT) method. An X-ray photoelectron spectrometer (XPS, ESCALAB250xi, Thermo Scientific) equipped with an Al K α X-ray source (1486.6 eV) was utilized to analyze the chemical composition of the powders. The Si 2p peaks of the

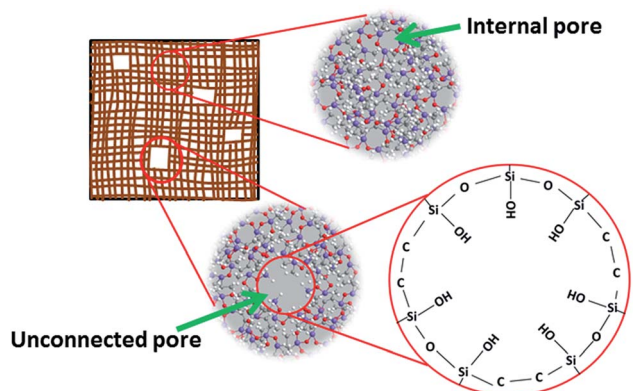


Fig. 1 Schematic illustration of two types of pore in organosilica networks derived from BTESE.

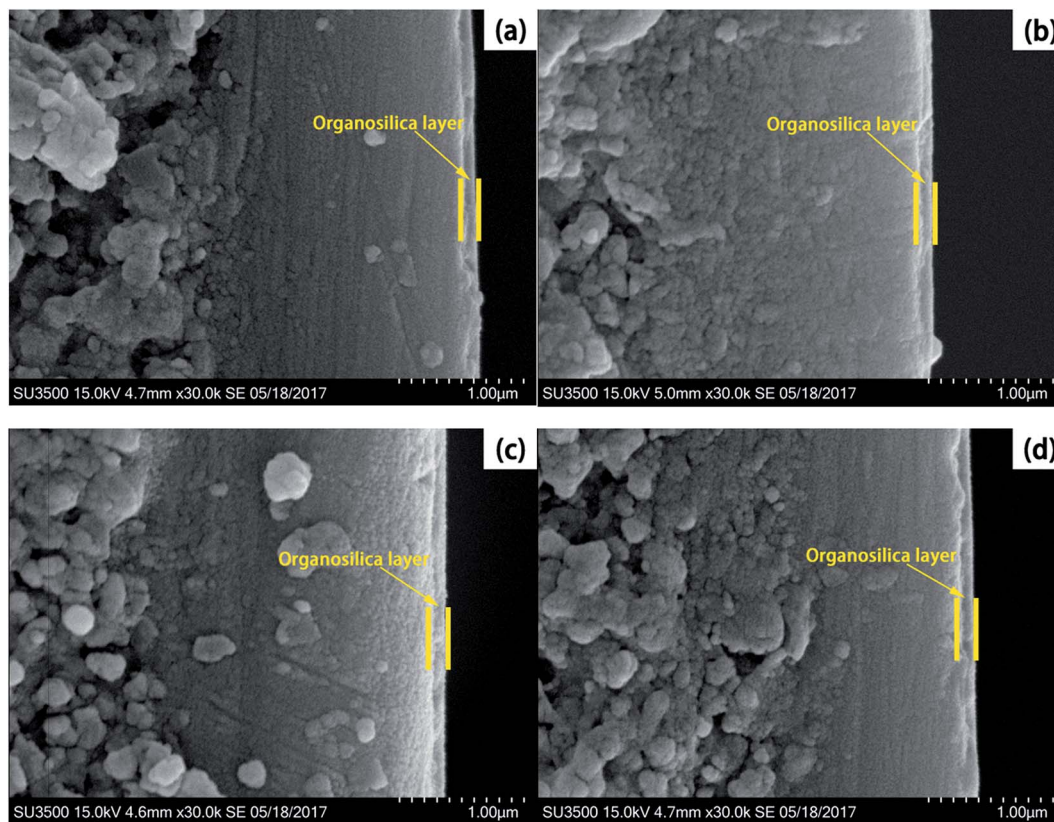


Fig. 2 Cross-sectional SEM images of the (a) M1, (b) M2, (c) M3 and (d) M4 membranes.

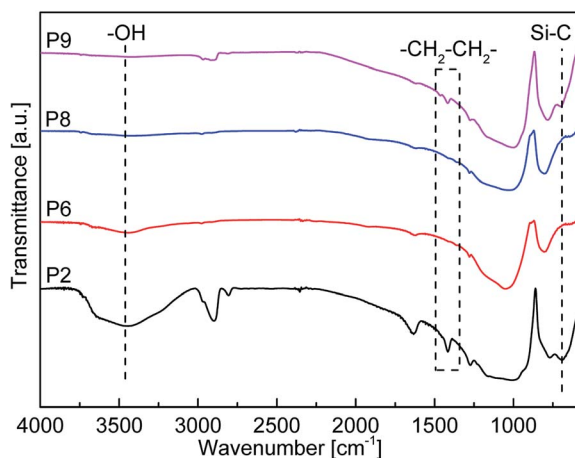


Fig. 3 FTIR spectra of the P2, P6, P8 and P9 powders.

organosilica powders were deconvoluted by the software package (XPSPEAK41) and relevant details are presented in Table S2.†

Scanning electron microscopy (SEM SU3500, Hitachi) was performed to study the morphology of the membrane cross-sections at an acceleration voltage of 15 kV. The gas separation performance of the as-prepared organosilica membranes was measured on a home-made permeance apparatus. The single gas permeances of He, H₂, CO₂, N₂, CH₄ and SF₆ were

obtained at a temperature range of 100–200 °C and repeat experiments of the gas permeances were conducted 9 times. The pressure difference through the membranes was maintained at 0.3 MPa. The gas permeance (P) was calculated by the formula:

$$P_i = \frac{F_i}{A\Delta P}$$

where P_i is the permeance of gas i ($\text{mol m}^{-2} \text{s}^{-1} \text{Pa}^{-1}$), F_i is the molar flow rate (mol s^{-1}), A is the effective membrane area (m^2), and ΔP is the transmembrane pressure (Pa).

The ideal separation factor (α , *i.e.* permselectivity) was defined as follows:

$$\alpha = \frac{P_i}{P_j}$$

where P_i and P_j are the permeance values for components i and j , respectively.

The activation energies (E_a) for H₂ and CO₂ permeating through the membranes were obtained by regressing the following equation:

$$P = P_0 \exp\left\{-\frac{E_a}{RT}\right\}$$

where P_0 is a temperature independent coefficient and T is the test temperature.

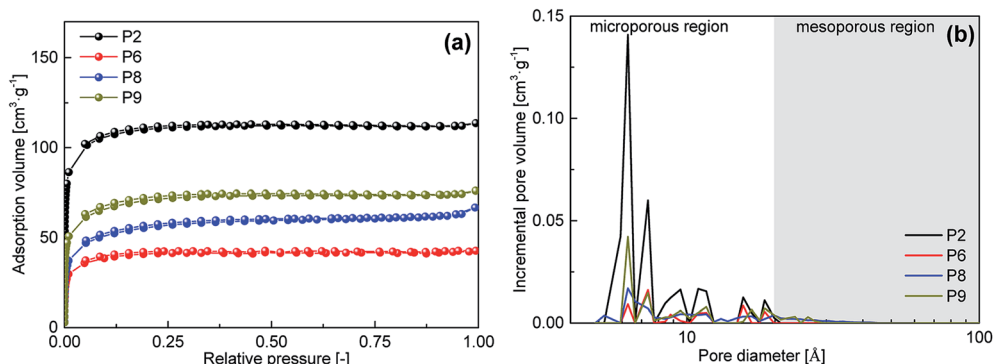


Fig. 4 (a) N_2 adsorption–desorption isotherms and (b) pore size distributions of P2, P6, P8 and P9 powders.

3. Results and discussion

3.1. Characterization of BTESE-derived organosilica membranes

As discussed above, the sol–gel process plays a crucial role in the preparation of high performance organosilica membranes. A series of BTESE-derived organosilica gel powders were prepared to determine the chemical states and the pore structures of the organosilica network. Details can be found in the ESI.† Based on these organosilica networks obtained by different calcination conditions, four organosilica membranes (M1, M2, M3 and M4) were prepared accordingly under the same calcination conditions used for the preparation of powders P2, P6, P8 and P9.

Fig. 2 shows the cross-sectional SEM images of the four as-prepared organosilica membranes. These organosilica membranes exhibit an asymmetric structure with an ultrathin separation layer (*i.e.* the organosilica layer) and an intermediate layer on top of the support. The separation layers of the four membranes have a similar thickness of about 100 nm irrespective of the calcination conditions.

Fig. 3 shows the FTIR spectra of the P2, P6, P8 and P9 powders which indirectly reflect the chemical structures of the organosilica networks in the M1, M2, M3 and M4 membranes. It can be seen that a notable absorption band at around 1020 cm^{-1} appears in all four organosilica powders which is assigned to the asymmetric stretching vibration of Si–O–Si groups.^{25,26} This is a typical characteristic of silica based

materials.^{25,26} The broad absorption band at 3450 cm^{-1} can be ascribed to the stretching vibrations of hydroxyl groups in the silanol groups (Si–OH).^{25,26} It is well known that silanol groups would condense to form a Si–O–Si network (*i.e.* dehydroxylation process) during the calcination process. Moreover, a higher calcination temperature leads to an enhanced dehydroxylation process (namely, a relatively higher cross-linking degree of the silica network). As shown in Fig. 3, the signal peak for Si–OH is obvious when the calcination temperature is $400\text{ }^\circ\text{C}$ (powder P2), but the peak for Si–OH disappears when the calcination temperature increases to $600\text{ }^\circ\text{C}$ using the same heating rate and dwelling time (powder P6). The intensity of the signal peak for Si–OH decreases with the increase of the calcination temperature, and it becomes negligible when the calcination temperature is above $500\text{ }^\circ\text{C}$ (Fig. S1a†). More details about the effects of calcination temperature on the chemical structure of the organosilica powders can be seen in Fig. S1.†

The peaks at 1410 cm^{-1} can be ascribed to CH_2 (in Si– CH_2 – CH_2 –Si) asymmetric bending vibrations and the peaks at approximately 700 cm^{-1} are assigned to Si–C stretching vibrations.^{26–28} The above-mentioned peaks are clearly detected in the spectrum of powder P2, while no vibration peaks at 700 and 1410 cm^{-1} are observed in the spectra of powders P6 and P8. This suggests that the thermal degradation of the organic bridge groups in the organosilica powders occurs at higher calcination temperatures. This is attributed to the thermally-sensitive nature of organic groups. In fact, when a slow calcination ($r = 0.5\text{ }^\circ\text{C min}^{-1}$, $t = 180\text{ min}$) is implemented,

Table 1 Pore structure data of organosilica powders calcined under different calcination conditions^a

Powder	Thermal treatment parameters			S_{BET} ($\text{m}^2\text{ g}^{-1}$)	V_{total} ($\text{cm}^3\text{ g}^{-1}$)	V_{micro} ($\text{cm}^3\text{ g}^{-1}$)	$V_{\text{micro}}/V_{\text{total}}$ (%)
	T_c ($^\circ\text{C}$)	r ($^\circ\text{C min}^{-1}$)	t (min)				
P2	400	0.5	180	338	0.173	0.140	80.9
P6	600	0.5	180	122	0.060	0.048	80.0
P8	600	10	180	178	0.097	0.050	51.5
P9	600	10	5	222	0.114	0.073	75.3

^a T_c , r , t , S_{BET} , V_{total} , V_{micro} and $V_{\text{micro}}/V_{\text{total}}$ represent calcination temperature, heating rate, dwelling time, BET specific surface area, total pore volume, micropore volume and microporosity, respectively.

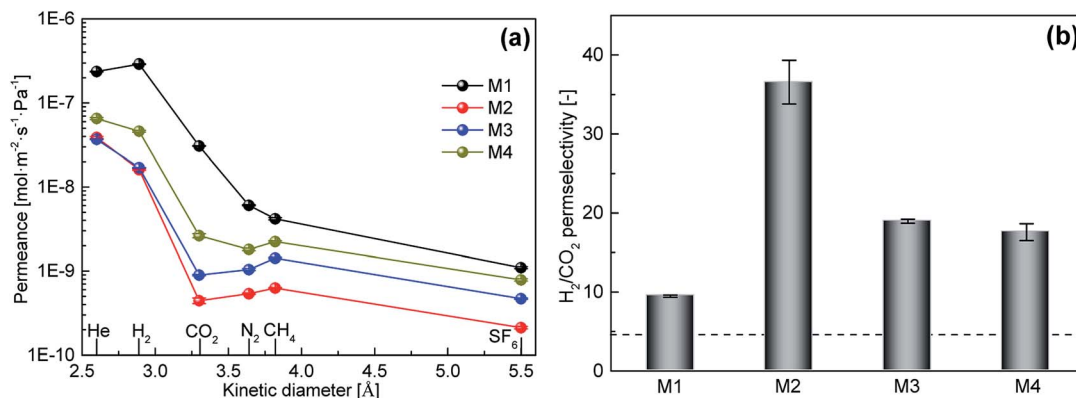


Fig. 5 (a) Gas permeance and (b) H_2/CO_2 permselectivity of M1, M2, M3 and M4 membranes. The dotted line in figure (b) represents the Knudsen diffusion factor with respect to H_2/CO_2 .

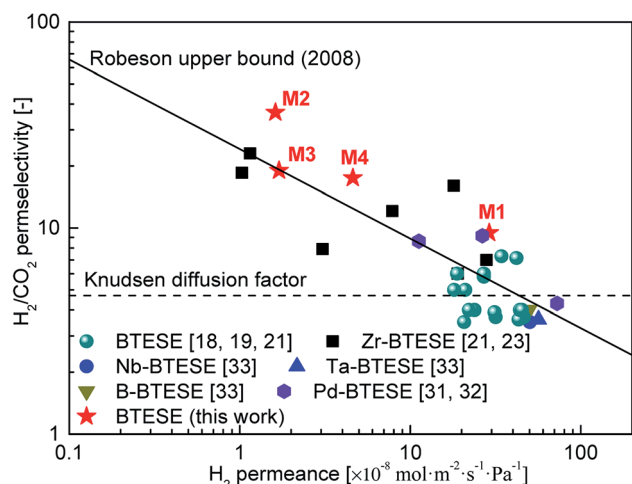


Fig. 6 Performance comparison of the M1, M2, M3 and M4 membranes with other organosilica membranes reported in the literature under a testing temperature of 200 °C.

a majority of the organic bridge groups in the organosilica powders have decomposed as the calcination temperature is equal to or higher than 500 °C. This change trend can be seen in

the decreasing intensity of the peaks at 700 and 1410 cm^{-1} in Fig. S1a.† The pyrolysis of the organic bridge groups is also confirmed by the color change of the organosilica powders (Fig. S2a†). It is obvious that the color of the organosilica powders turns gradually from white to yellow when the calcination temperature increases.

There is no distinguished difference in the FTIR absorption spectra of powders P6 ($r = 0.5 \text{ } ^\circ C \text{ min}^{-1}$) and P8 ($r = 10 \text{ } ^\circ C \text{ min}^{-1}$), indicating that the organic bridge groups decompose under these conditions ($T = 600 \text{ } ^\circ C$, $t = 180 \text{ min}$) regardless of the heating rates. Additional details about the effects of the heating rate on the chemical structure and appearance of the organosilica powders are shown in Fig. S1b and S2b.† All samples show a high cross-linking degree of the silica network since negligible peaks of the silanol groups are observed in the corresponding FTIR spectra (Fig. S1b†). The absence of the FTIR absorption peaks at 700 and 1410 cm^{-1} and the yellow color of the organosilica powders indicate that most organic bridge groups have decomposed under these conditions.

The organosilica powders calcined at 600 °C with a heating rate of 10 $^\circ C \text{ min}^{-1}$ and a dwelling time of 5 min (powder P9) show no obvious peak at 3450 cm^{-1} . But obvious peaks at 700

Table 2 Comparison of the as-prepared membranes in this work with other reported inorganic membranes in terms of H_2/CO_2 separation performance

Membrane materials	Test temperature (°C)	H_2 permeance ($\text{mol m}^{-2} \text{ s}^{-1} \text{ Pa}^{-1}$)	H_2/CO_2 permselectivity [-]	References
Pd	150	2.93×10^{-8a}	22.3	35
Carbon	Ambient	2.7×10^{-8}	14.2	36
MoS ₂	35	8.19×10^{-7}	4.4	37
ZSM-5	500	1.2×10^{-7}	23	39
ZIF-7	220	4.55×10^{-8}	13	40
ZIF-90	200	2.5×10^{-7}	7.2	41
SiO ₂	200	5×10^{-7}	70	2
M1	200	2.92×10^{-7}	9.47	This work
M2	200	1.62×10^{-8}	36.4	This work
M3	200	1.7×10^{-8}	19	This work
M4	200	4.61×10^{-8}	17.5	This work

^a This value is expressed in permeability (barrer) in the literature, 1 barrer = $1 \times 10^{-10} \text{ cm}^3(\text{STP}) \text{ cm cm}^{-2} \text{ s}^{-1} \text{ cm Hg}^{-1}$.

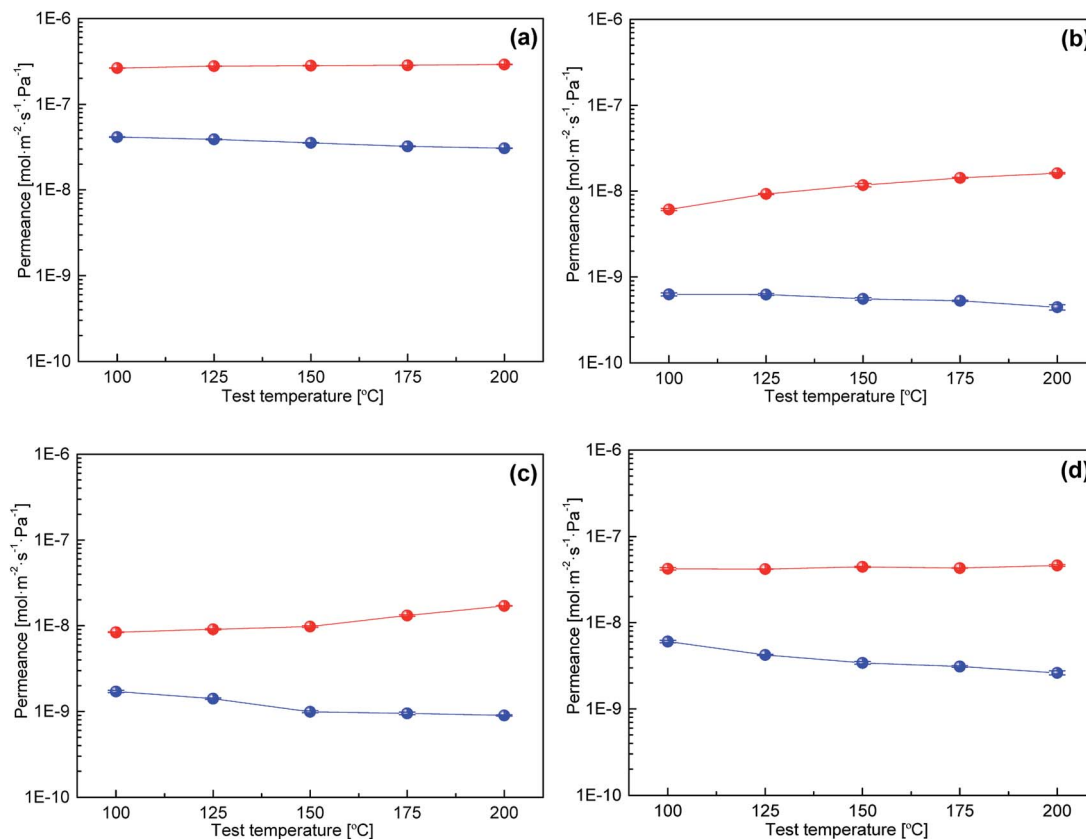


Fig. 7 Temperature dependence of H₂ (red) and CO₂ (blue) permeances of the (a) M1, (b) M2, (c) M3 and (d) M4 membranes.

and 1410 cm⁻¹ are detected for powder P9. Furthermore, FTIR absorption spectra of organosilica powders calcined at 600 °C with a heating rate of 10 °C min⁻¹ and various dwelling times are displayed in Fig. S1c.† All samples show negligible silanol peaks. Interestingly, the signal peaks of the organic bridge groups appear when the dwelling time reduces to 10 min and the signal intensity becomes stronger as the dwelling time continues to decrease. Notably, organosilica powders show a white color when the dwelling time is equal to or less than 10 min (Fig. S2c.†). This indicates that a silica network structure with a high cross-linking degree and with organic bridge groups can be obtained using an expeditious calcination, even at 600 °C.

N₂ adsorption–desorption measurements at 77 K were conducted on organosilica powders to probe the pore structure of the corresponding organosilica membranes. Fig. 4a describes

Table 4 The pore sizes of the organosilica membranes obtained from the normalized Knudsen-based permeance (NKP) method

Membrane	Pore size (Å)
M1	4.54
M2	3.62
M3	3.78
M4	4.03

the N₂ adsorption–desorption isotherms of the P2, P6, P8 and P9 powders. All samples exhibit type I isotherms that correspond to microporous structures.²⁹ The pore structure data derived from the N₂ adsorption–desorption results are displayed in Table 1. It can be seen that the organosilica powders

Table 3 Apparent activation energies (E_a) for gas permeation through the organosilica membranes

Membrane	Calcination conditions			E_{a,H_2} (kJ mol ⁻¹)	E_{a,CO_2} (kJ mol ⁻¹)
	T_c (°C)	r (°C min ⁻¹)	t (min)		
M1	400	0.5	180	1.29	-4.61
M2	600	0.5	180	14.19	-4.93
M3	600	10	180	10.27	-10.09
M4	600	10	5	1.12	-11.81

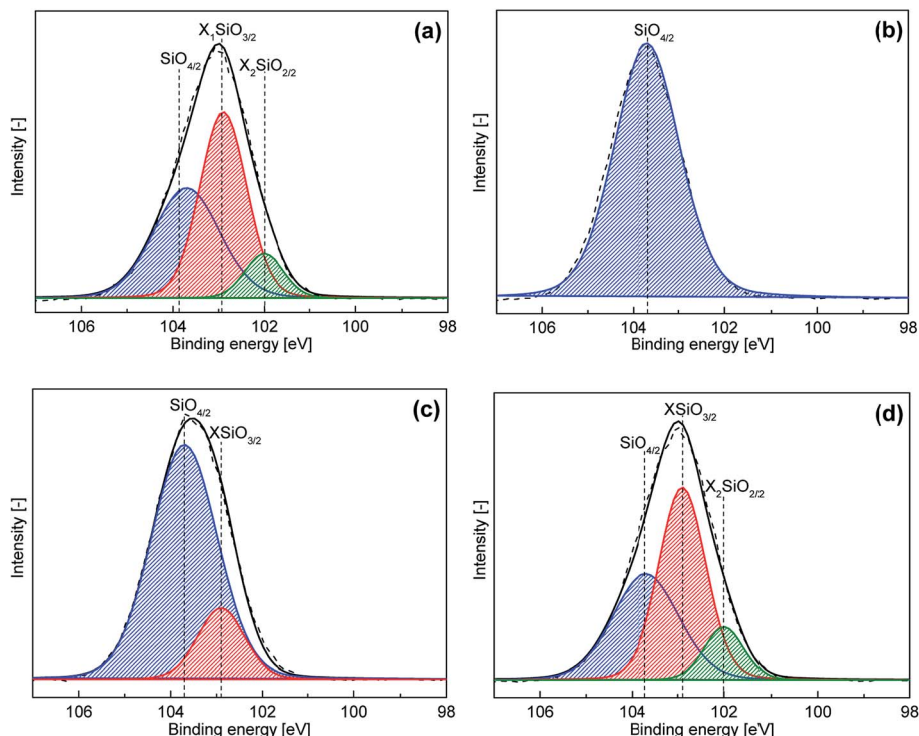


Fig. 8 Deconvolutions of the XPS Si 2p peaks of the (a) P2, (b) P6, (c) P8 and (d) P9 powders.

calcined at 400 °C (powder P2) have a Brunauer–Emmett–Teller (BET) surface area of 338 m² g⁻¹ and a pore volume of 0.173 cm³ g⁻¹. When the calcination temperature rises to 600 °C, the BET surface area and pore volume of the organosilica powders (powder P6) dramatically decrease to 122 m² g⁻¹ and 0.06 cm³ g⁻¹, respectively. These results suggest that the organosilica powders calcined at higher temperatures have denser structures. And these results are in line with previous reports for silica membranes.²⁴ In contrast, when the calcination

temperature is 600 °C and the dwelling time is 180 min, the gas adsorption capacity, BET surface area and pore volume of the organosilica powders increase with the increase of the heating rate from 0.5 to 10 °C min⁻¹ (powders P6 and P8). Additionally, when the calcination temperature is 600 °C and the heating rate is 10 °C min⁻¹, the organosilica powders (P8 and P9) show increases in the BET surface area (from 178 to 222 m² g⁻¹) and pore volume (from 0.097 to 0.114 cm³ g⁻¹) as the dwelling time decreases from 180 to 5 min. Table S1† shows more details

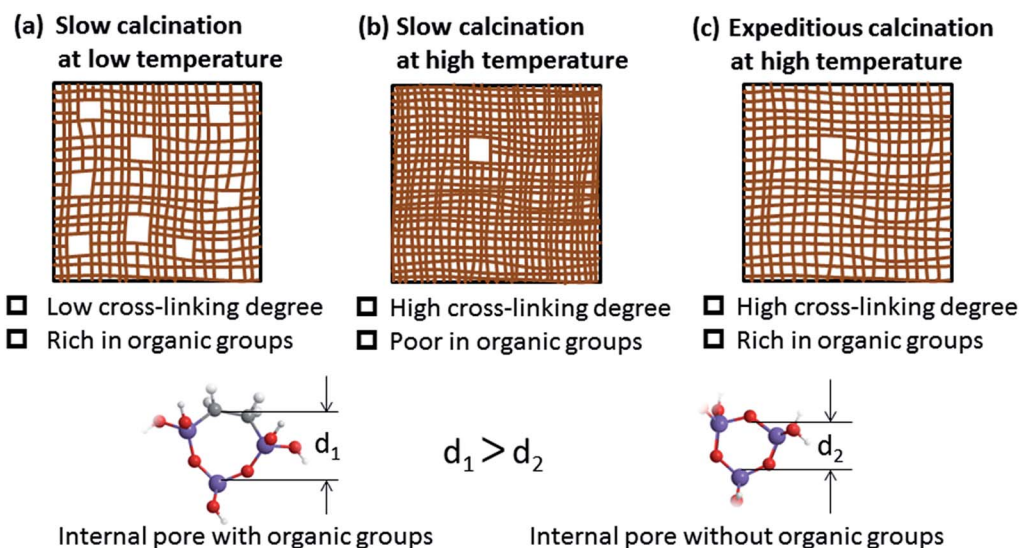


Fig. 9 Schematic illustration of the BTESE-derived organosilica membranes calcined under different calcination conditions.

about the effects of the calcination parameters on the pore structure of the BTESE-derived organosilica powders.

To further explore the pore structure of the as-prepared membranes, the pore size distributions of the P2, P6, P8 and P9 powders were analyzed using the NLDFT method and are displayed in Fig. 4b. Obviously, all samples have multimodal pore size distributions. This is ascribed to the hierarchically porous structure of organosilica (as shown in Fig. 1). This hierarchically porous characteristic of organosilica is similar to that of typical sol-gel derived silica.^{1,30} The internal pores (also known as intraparticle pores by Tsuru¹) in pure silica are formed by the Si–O–Si network structure while the internal pores in organosilica are formed by a Si–O–Si and Si–CH₂–CH₂–Si hybrid structure. It is believed that small molecules such as helium and hydrogen can permeate through these internal pores while larger molecules fail to pass through.¹ As a result, both silica and organosilica membranes show H₂- and He-selective properties. Unconnected pores (also known as interparticle pores¹) are generated as voids between sol/gel particles. Because large molecules can permeate through these pores, they have negative effects on membrane selectivity. Therefore, in order to improve H₂ selectivity, the undesirable unconnected pores should be eliminated within the structure rather than linked together. It is worth noting that the majority of pores in organosilica powders are micropores (pore size < 20 Å). By changing the calcination temperature from 400 to 600 °C, the organosilica powders show a dramatic decrease in the pore volume. Conversely, the pore volume of organosilica powders increases with the increase of the heating rate from 0.5 to 10 °C min⁻¹. However, the pore size distributions of organosilica powders are broadened by increasing the heating rate. This may result in lower permselectivities of the corresponding membrane. From Fig. 4b, it can also be deduced that the pore volume of organosilica powders increases when the dwelling time reduces from 180 to 5 min.

3.2 Gas separation performance of BTESE-derived organosilica membranes

Fig. 5a displays the single gas permeances of organosilica membranes under a test temperature of 200 °C. It can be seen that all four membranes show much higher permeances for H₂ (kinetic diameter: 2.89 Å) and He (kinetic diameter: 2.6 Å) than for other gases with larger kinetic diameters, indicating that all membranes have high H₂ and He permeabilities. This is because small gas molecules (H₂ and He) can permeate through both the internal and the unconnected pores, while larger gas molecules permeate only through the unconnected pores which have a relatively larger size. Obviously, the membrane calcined at 400 °C has much higher gas permeance than the membranes calcined at 600 °C. For example, the H₂ permeance of membrane M1 is as high as 2.90×10^{-7} mol m⁻² s⁻¹ Pa⁻¹, while the H₂ permeance of membrane M2 is 1.62×10^{-8} mol m⁻² s⁻¹ Pa⁻¹. This indicates that membrane M2 has a denser pore structure than that of membrane M1. On the other hand, the H₂ permeance of membrane M3 is a little higher than that of M2 (1.70 vs. 1.62×10^{-8} mol m⁻² s⁻¹ Pa⁻¹) while the CO₂, N₂,

CH₄ and SF₆ permeance of M3 is much higher than that of membrane M2. This indicates that membrane M3 has more unconnected pores through which CO₂, N₂, CH₄ and SF₆ molecules can pass through. Furthermore, membrane M4 prepared by an expeditious calcination at 600 °C has a higher H₂ permeance than membrane M3 (4.61×10^{-8} vs. 1.70×10^{-8} mol m⁻² s⁻¹ Pa⁻¹), suggesting that membrane M4 has a looser pore structure than that of membrane M3.

Fig. 5b presents the H₂/CO₂ permselectivities of the as-prepared organosilica membranes. It can be seen that all four membranes have good H₂/CO₂ permselectivities (9.47, 36.4, 19.0 and 17.5 for membranes M1, M2, M3 and M4, respectively), which are higher than the corresponding Knudsen diffusion factor. Up to now, most BTESE-derived membranes reported in the literature show moderate H₂/CO₂ selectivity (close to the corresponding Knudsen diffusion factor of 4.69). Our membranes exhibit extraordinary molecular sieving properties for H₂/CO₂. Fig. 6 presents the performance comparison with respect to H₂ permeance and H₂/CO₂ permselectivity of our membranes and other reported BTESE-derived membranes (test temperature: 200 °C).^{18,19,21,23,31–33} It can be seen that the H₂/CO₂ permselectivities of the organosilica membranes in this work are higher than those of other pure BTESE membranes. In addition, the H₂/CO₂ separation performances of membranes M1, M2 and M4 exceed the Robeson upper bound.³⁴ Besides organosilica membranes, numerous membranes have been used for gas separation.^{35–41} Table 2 compares the H₂ permeance and permselectivity of our organosilica membranes with those of other types of membrane, including Pd,³⁵ carbon molecular sieve,³⁶ MoS₂,³⁷ ZSM-5,³⁹ ZIF-7,⁴⁰ ZIF-90 (ref. 41) and SiO₂ (ref. 2) membranes. It is apparent that there is an inevitable trade-off between the H₂ permeance and the H₂/CO₂ permselectivity for all membranes. For instance, the MoS₂ membrane has a H₂ permeance as high as 8.19×10^{-7} mol m⁻² s⁻¹ Pa⁻¹, but it has a low H₂/CO₂ permselectivity of 4.4 which is close to the corresponding Knudsen diffusion factor (4.69),³⁷ while the Pd membrane shows a good H₂/CO₂ sieving capability but a relative low H₂ permeance.³⁵ It is noteworthy that the SiO₂ membrane shows outstanding H₂/CO₂ separation performance,² however, it has been proven to be unstable in hydrothermal conditions. Therefore, compared with other inorganic membranes, the as-prepared organosilica membranes are relatively competitive in H₂/CO₂ separation performance.

The temperature dependence of gas permeance is of great importance to gas transport behaviour which is closely related to the pore structures of the membranes. Therefore, the H₂ and CO₂ permeances of organosilica membranes were measured at different testing temperatures. Fig. 7 shows the temperature dependence of gas permeance for the four membranes. For all organosilica membranes, H₂ permeances show an upward tendency varying with the increase of the testing temperature, while CO₂ permeances show a downward tendency with increasing testing temperatures. The apparent activation energies for H₂ and CO₂ permeation through the organosilica membranes are summarized in Table 3. All apparent activation energies for H₂ are positive, which suggests that H₂ molecules pass through our membranes by activated diffusion.⁴² In

general, a higher activation energy is required to permeate through denser pores since higher repulsive forces must be conquered by the molecules in denser pores. We also found that the apparent activation energies for H₂ molecules through the M2 and M3 membranes are much higher than those of membranes M1 and M4. This indicates that membranes M1 and M4 have looser pore structures than those of membranes M2 and M3. The different pore structures of the organosilica membranes may be attributed to the cross-linking degree of the silica network and the amount of organic bridge groups. It should be noted that all four membranes have negative apparent activation energies for CO₂ permeation, suggesting that the transport of the CO₂ molecule through the organosilica membrane is dominated by an adsorption-based mechanism (*i.e.* surface diffusion).

We also applied the normalized Knudsen-based permeance (NKP) method⁴³ to calculate the effective pore size of the organosilica membranes. A brief introduction of the NKP method can be found in the ESI.† The calculated pore sizes of the organosilica membranes are presented in Table 4. The effective pore sizes are estimated to be 4.54, 3.62, 3.78 and 4.03 Å for membranes M1, M2, M3 and M4, respectively, which are consistent with the results discussed above.

3.3 Tailoring the pore structure by tuning the calcination parameters

To quantitatively analyze the structure of the organosilica membranes calcined under different conditions, XPS analysis is conducted on the corresponding organosilica powders. Deconvolutions of XPS Si 2p peaks are shown in Fig. 8 and the deconvolution details are provided in Table S2.† For powder P2, the Si 2p peak can be decoupled into three peaks (103.7, 102.9, and 102 eV) corresponding to SiO_{4/2}, XSiO_{3/2} and X₂SiO_{2/2} (X represents organic groups) in the organosilica powders.²⁶ The content of SiO_{4/2}, XSiO_{3/2} and X₂SiO_{2/2} is 41.1%, 49.1% and 9.8%, respectively. The sole peak at 103.7 eV in the spectrum of powder P6 corresponds to the inorganic moieties, suggesting that the organic moieties have been decomposed completely. These results agree with the above-mentioned FTIR results. For powder P8, the Si 2p peaks can be decoupled into two peaks corresponding to SiO_{4/2} (82.3%) and XSiO_{3/2} (17.7%), while the peaks of the organic moieties are observed in the spectrum of powder P9. Moreover, the amounts of XSiO_{3/2} and X₂SiO_{2/2} reach 49.7% and 11.4%, respectively.

Based on the results and discussion above, the difference in the pore structure of organosilica membranes calcined with various calcination parameters is schematically illustrated in Fig. 9. The BTESE-derived organosilica membrane calcined with a slow calcination process at low temperature (*e.g.* $T_c = 400$ °C, $r = 0.5$ °C min⁻¹ and $t = 180$ min) shows a low cross-linking degree of the silica network and a high amount of organic bridge groups (Fig. 9a). A slow calcination at higher temperature (*e.g.* $T_c = 600$ °C, $r = 0.5$ and 10 °C min⁻¹, $t = 180$ min) leads to a high cross-linking degree but to much destruction of the organic bridge groups (Fig. 9b). An expeditious calcination causes a high cross-linking degree without much destruction of

the organic bridge groups in the BTESE-derived organosilica network (Fig. 9c). Both the cross-linking degree of the silica network and the amount of organic bridge groups have significant effects on the pore structure of the organosilica membranes. On the one hand, a higher cross-linking degree results in a denser pore structure. On the other hand, organosilica membranes with a higher amount of organic bridge groups have looser structures. Molecular dynamics simulations and numerous experimental studies^{17,44–46} have confirmed that organosilica membranes have looser networks than pure inorganic silica membranes due to the space effect of the organic bridge groups between the Si atoms. The space effect of the organic bridge groups on the internal pores of the network structure is also graphically presented in Fig. 9. The size of the internal pores decreases (from d_1 to d_2) when the organic bridge groups are removed from the network structure.

It can be deduced that the organosilica membrane prepared at a low temperature shows high H₂ permeance but moderate H₂/CO₂ permselectivity. The organosilica membrane calcined at a high temperature with a slow calcination has low permeance but high permselectivity. Notably, based upon an expeditious calcination at a high temperature, the organosilica membrane can simultaneously display good H₂ permeance and H₂/CO₂ permselectivity.

4. Conclusions

A series of BTESE-derived organosilica powders were prepared under different calcination conditions and used to investigate the effects of calcination parameters on the organosilica pore structures. Four BTESE-derived organosilica membranes were prepared based upon four typical calcination conditions. The microstructure and H₂/CO₂ separation performance of the as-prepared membranes were studied. It is found that tuning the calcination parameters can tailor the pore structures of the BTESE-derived organosilica membranes and consequently improve the H₂/CO₂ separation performance, especially the permselectivity. The mechanism behind this result was further investigated and presented. The following conclusions can be drawn.

(1) The organosilica membrane calcined at 400 °C with a slow calcination process ($r = 0.5$ °C min⁻¹, $t = 180$ min) shows a moderate H₂/CO₂ permselectivity (9.47). Increasing the calcination temperature to 600 °C results in a significant improvement in H₂/CO₂ permselectivity (up to 36.4) but a reduction in H₂ permeance (a decrease from 2.92×10^{-7} to 1.62×10^{-8} mol m⁻² s⁻¹ Pa⁻¹) when the heating rate and dwelling time remain the same. The organosilica membrane calcined with an expeditious calcination ($r = 10$ °C min⁻¹, $t = 5$ min) at 600 °C shows a H₂ permeance of 4.61×10^{-8} mol m⁻² s⁻¹ Pa⁻¹ and a H₂/CO₂ permselectivity of 17.5.

(2) The organic bridge groups in organosilica are sensitive to the calcination conditions. The organic bridge groups decompose when the samples are calcined at a high temperature for a relatively long time, while an expeditious calcination results in less destruction of the organic bridge groups. The amount of organic bridge groups is closely related to the pore structure of the organosilica membranes, as evidenced by the fact that

a higher content of organic bridge groups leads to more porous structures yielding higher H₂ permeances, accordingly.

Conflicts of interest

There are no conflicts of interest to declare.

Acknowledgements

This work is supported by the National Natural Science Foundation of China (21490581 and 21276123), the National High Technology Research and Development Program of China (2012AA03A606) and the “Summit of the Six Top Talents” Program of Jiangsu Province (2011-XCL-021).

References

- 1 T. Tsuru, *J. Sol-Gel Sci. Technol.*, 2008, **46**, 349–361.
- 2 R. M. de Vos, *Science*, 1998, **279**, 1710–1711.
- 3 J. Sekulić, M. W. J. Luiten, J. E. ten Elshof, N. E. Benes and K. Keizer, *Desalination*, 2002, **148**, 19–23.
- 4 B. Bettens, S. Dekeyzer, B. Van der Bruggen, J. Degève and C. Vandecasteele, *J. Phys. Chem. B*, 2005, **109**, 5216–5222.
- 5 J. Dong, Y. S. Lin, M. Kanezashi and Z. Tang, *J. Appl. Phys.*, 2008, **104**, 121301.
- 6 M. Pera-Titus, *Chem. Rev.*, 2014, **114**, 1413–1492.
- 7 N. W. Ockwig and T. M. Nenoff, *Chem. Rev.*, 2007, **107**, 4078–4110.
- 8 R. M. de Vos, W. F. Maier and H. Verweij, *J. Membr. Sci.*, 1999, **158**, 277–288.
- 9 M. C. Duke, J. C. D. da Costa, D. D. Do, P. G. Gray and G. Q. Lu, *Adv. Funct. Mater.*, 2006, **16**, 1215–1220.
- 10 D. Uhlmann, S. Liu, B. P. Ladewig and J. C. Diniz da Costa, *J. Membr. Sci.*, 2009, **326**, 316–321.
- 11 H. S. Choi, C. H. Ryu and G. J. Hwang, *Chem. Eng. J.*, 2013, **232**, 302–309.
- 12 G. Q. Lu, J. C. Diniz da Costa, M. Duke, S. Giessler, R. Socolow, R. H. Williams and T. Kreutz, *J. Colloid Interface Sci.*, 2007, **314**, 589–603.
- 13 R. Xu, S. M. Ibrahim, M. Kanezashi, T. Yoshioka, K. Ito, J. Ohshita and T. Tsuru, *ACS Appl. Mater. Interfaces*, 2014, **6**, 9357–9364.
- 14 H. L. Castricum, G. G. Paradis, M. C. Mittelmeijer-Hazeleger, R. Kreiter, J. F. Vente and J. E. ten Elshof, *Adv. Funct. Mater.*, 2011, **21**, 2319–2329.
- 15 M. Kanezashi, Y. Yoneda, H. Nagasawa, T. Tsuru, K. Yamamoto and J. Ohshita, *AIChE J.*, 2017, **63**, 4491–4498.
- 16 H. L. Castricum, A. Sah, R. Kreiter, D. H. A. Blank, J. F. Vente and J. E. ten Elshof, *Chem. Commun.*, 2008, 1103–1105.
- 17 M. Kanezashi, K. Yada, T. Yoshioka and T. Tsuru, *J. Am. Chem. Soc.*, 2009, **131**, 414–415.
- 18 H. F. Qureshi, A. Nijmeijer and L. Winnubst, *J. Membr. Sci.*, 2013, **446**, 19–25.
- 19 H. L. Castricum, H. F. Qureshi, A. Nijmeijer and L. Winnubst, *J. Membr. Sci.*, 2015, **488**, 121–128.
- 20 H. Qi, J. Han, N. P. Xu and H. J. M. Bouwmeester, *ChemSusChem*, 2010, **3**, 1375–1378.
- 21 M. ten Hove, A. Nijmeijer and L. Winnubst, *Sep. Purif. Technol.*, 2015, **147**, 372–378.
- 22 H. Song, Y. Wei, C. Wang, S. Zhao and H. Qi, *Chin. J. Chem. Eng.*, DOI: 10.1016/j.cjche.2017.04.010.
- 23 H. Song, S. Zhao, J. Chen and H. Qi, *Microporous Mesoporous Mater.*, 2016, **224**, 277–284.
- 24 M. Kanezashi, T. Sasaki, H. Tawarayama, H. Nagasawa, T. Yoshioka, K. Ito and T. Tsuru, *J. Phys. Chem. C*, 2014, **118**, 20323–20331.
- 25 A. P. Dral, K. Tempelman, E. J. Kappert, L. Winnubst, N. E. Benes and J. E. ten Elshof, *J. Mater. Chem. A*, 2017, **5**, 1268–1281.
- 26 P. H. T. Ngamou, J. P. Overbeek, R. Kreiter, H. M. van Veen, J. F. Vente, I. M. Wienk, P. F. Cuperus and M. Creatore, *J. Mater. Chem. A*, 2013, **1**, 5567–5576.
- 27 H. Nagasawa, M. Nishibayashi, M. Kanezashi, T. Yoshioka and T. Tsuru, *RSC Adv.*, 2017, **7**, 7150–7157.
- 28 K. Yamamoto, J. Ohshita, T. Mizumo and T. Tsuru, *J. Non-Cryst. Solids*, 2015, **408**, 137–141.
- 29 K. K. Matthias Thommes, A. V. Neimark, J. P. Olivier, F. Rodriguez-Reinoso, J. Rouquerol and K. S. W. Sing, *Pure Appl. Chem.*, 2015, **87**, 1051–1069.
- 30 M. C. Duke, S. J. Pas, A. J. Hill, Y. S. Lin and J. C. D. da Costa, *Adv. Funct. Mater.*, 2008, **18**, 3818–3826.
- 31 J. Lei, H. Song, Y. Wei, S. Zhao and H. Qi, *Microporous Mesoporous Mater.*, 2017, **253**, 55–63.
- 32 H. Song, S. Zhao, J. Lei, C. Wang and H. Qi, *J. Mater. Sci.*, 2016, **51**, 6275–6286.
- 33 H. F. Qureshi, R. Besselink, J. E. ten Elshof, A. Nijmeijer and L. Winnubst, *J. Sol-Gel Sci. Technol.*, 2015, **75**, 180–188.
- 34 L. M. Robeson, *J. Membr. Sci.*, 2008, **320**, 390–400.
- 35 S. Y. Kong, D. H. Kim, D. Henkensmeier, H. J. Kim, H. C. Ham, J. Han, S. P. Yoon, C. W. Yoon and S. H. Choi, *Sep. Purif. Technol.*, 2017, **179**, 486–493.
- 36 S. Roy, R. Das, M. K. Gagrai and S. Sarkar, *J. Porous Mater.*, 2016, **23**, 1653–1662.
- 37 D. Wang, Z. Wang, L. Wang, L. Hu and J. Jin, *Nanoscale*, 2015, **7**, 17649–17652.
- 38 V. I. Isaeva, M. I. Barkova, L. M. Kustov, D. A. Syrtsova, E. A. Efimova and V. V. Tepliyakov, *J. Mater. Chem. A*, 2015, **3**, 7469–7476.
- 39 H. Wang, X. Dong and Y. S. Lin, *J. Membr. Sci.*, 2014, **450**, 425–432.
- 40 Y. Li, F. Liang, H. Bux, W. Yang and J. Caro, *J. Membr. Sci.*, 2010, **354**, 48–54.
- 41 A. Huang, W. Dou and J. Caro, *J. Am. Chem. Soc.*, 2010, **132**, 15562–15564.
- 42 T. Yoshioka, E. Nakanishi, T. Tsuru and M. Asaeda, *AIChE J.*, 2001, **47**, 2052–2063.
- 43 H. Nagasawa, T. Niimi, M. Kanezashi, T. Yoshioka and T. Tsuru, *AIChE J.*, 2014, **60**, 4199–4210.
- 44 K. S. Chang, T. Yoshioka, M. Kanezashi, T. Tsuru and K. L. Tung, *Chem. Commun.*, 2010, **46**, 9140–9142.
- 45 M. Kanezashi, K. Yada, T. Yoshioka and T. Tsuru, *J. Membr. Sci.*, 2010, **348**, 310–318.
- 46 M. Kanezashi, M. Kawano, T. Yoshioka and T. Tsuru, *Ind. Eng. Chem. Res.*, 2012, **51**, 944–953.